JOURNAL OF GEOPHYSICAL RESEARCH, VOL. 102, NO. D8, PAGES 9359-9374, APRIL 27, 1997

Precipitation water path and rainfall rate estimates over oceans using special sensor microwave imager and International Satellite Cloud Climatology Project data

Bing Lin[1]
Hampton University, Hampton, Virginia

William B. Rossow
NASA Goddard Institute for Space Studies, New York

Abstract. The liquid/ice water paths (LWP/IWP) and the rainfall rate (RR) of precipitation systems over oceans are estimated using a combination of data from the special sensor microwave/imager (SSM/I) and the International Satellite Cloud Climatology Project (ISCCP). The retrieval scheme is based on microwave radiative transfer simulations. Collocated ISCCP cloud top temperatures are used to separate warm from cold precipitating clouds: cold precipitating clouds occur much more frequently than warm precipitating clouds and produce over 80% of the precipitation, but warm precipitating clouds are not negligible in the tropics and summer midlatitudes. SSM/I data are used to identify precipitating clouds: precipitating clouds are very rare (about 5% of all locations). Estimated IWP values, with mean about 7 mg/cm^2, are quite variable, ranging from as little as 5 mg/cm^2 to as much as 200 mg/cm^2. The mean LWP in precipitating clouds is approximately 80 mg/cm^2, occasionally reaching 1000 mg/cm^2. Average RR (both cold and warm) is about 1.5 mm/hr, generally larger in the tropics than in midlatitudes. RR is larger in the northern hemispheric midlatitudes than in the southern midlatitudes. The global annual cycle of precipitation is dominated by tropical variations and is in phase with boreal seasons. The largest annual total precipitation occurs in the eastern Pacific (about 5000 mm). The subtropical precipitation minima may be underestimated because drizzle does not produce strong microwave signals.

1. Introduction

There have been numerous investigations of methods to determine average total precipitation over oceans from satellite observations because of the importance of precipitation to surface salinity and deep ocean circulations [e.g., *Broecker*, 1987] and because of an almost complete lack of comprehensive surface observations [e.g., *Morrissey et al.*, 1995; *Legates and Willmott*, 1990; *Jaeger*, 1983; *Dorman and Bourke*, 1979, 1981]. The effect of precipitation on the ocean circulation arises from its global scale variations, so that the emphasis has been on microwave techniques that are more accurate both within and outside the tropics than "optical" methods [cf. *Liu and Curry*, 1992; *Negri et al.*, 1994, and references therein].

Microwave remote sensing methods usually combine a microwave radiative transfer model with a physical model of a precipitating cloud to estimate rainfall rate (RR) because the directly sensed quantity is total water path. All absorptions by gases and cloud water particles and scattering and absorption by precipitating liquid/ice hydrometeors are accounted for in the combined models [*Wilheit et al.*, 1977, 1991; *Olson*, 1987; *Wu and Weinman*, 1984; *Kummerow et al.*, 1989; *Liu and Curry*, 1992; *Kummerow and Giglio*, 1994a, b; *Petty*, 1994a, b; *Smith et al.*, 1992]. Precipitating hydrometeors (i.e., rain droplets, large ice crystals and graupel that are larger than about 150 μm) in raining cloud systems absorb and scatter microwave radiation, but scattering predominates when large ice crystals and graupel are present, especially at higher (>60 GHz) frequencies. Consequently, when ice precipitation is present aloft, microwave methods may not even directly observe the rain droplets below and have to estimate rainfall rates indirectly using a physical model of a precipitating cloud that relates column water amount to RR [*Adler et al.*, 1991; *Smith et al.*, 1992; *Mugnai et al.*, 1993].

Comparing almost all available satellite rainfall estimates (most from special sensor microwave/imager (SSM/I)) with ground observations (gauge and radar), *Barrett et al.* [1994] found that there are large differences among the satellite results, although the major large-scale features of the global distribution are qualitatively similar. One problem for these microwave algorithms is how to distinguish between and deal with deep and shallow convection. If the microwave analysis is limited to higher frequencies (>60 GHz) because the brightness temperatures are nearly linearly related to rainfall rates (actually to the column amounts of precipitation-sized ice particles) in deep convective and/or anvil clouds (i.e., cold precipitating clouds), the method cannot handle shallow, warm precipitating systems that lack ice precipitation [*Barrett*

[1]Also at NASA Langley Research Center, Hampton, Virginia.

Paper number 96JD03987.
0148-0227/97/96JD-03987$09.00

et al., 1994; *Janowiak et al.*, 1995]. If the analysis is based on lower frequencies, the water amounts in nonprecipitating clouds will distort the rainfall estimates [*Janowiak et al.*, 1995]. Moreover, the large field-of-view (FOV) of microwave instruments at lower frequencies and the nonlinear relationship between brightness temperature (Tb) and rainfall rate produce beam-filling problems [*Petty*, 1994a; *Chiu et al.*, 1990; *Short and North*, 1990]. These problems may explain why the various satellite methods produce considerable differences in the east Pacific Intertropical Convergence Zone (ITCZ), where the interactions between ITCZ and midlatitude cyclonic systems may promote substantial amounts of shallow convection, especially during northern hemisphere winter [*Janowiak et al.*, 1995].

In this study, collocated "optical" satellite measurements (i.e., visible and infrared radiances) are used to classify each SSM/I FOV into three categories: clear, warm-topped ($T > 0°C$) clouds, and cold-topped ($T \leq 0°C$) clouds. The SSM/I data are then used to separate the clouds into nonprecipitating clouds (both cold and warm), warm precipitating clouds, and cold precipitating clouds. We use the 85 GHz SSM/I data to estimate RR for cold precipitating clouds as done by *Adler et al.* [1993]. For warm precipitating clouds that are usually associated with weak precipitation, we find that RR is near linearly related to the polarization difference at 19.35 GHz as in the emission-based SSM/I rainfall algorithms [e.g., *Wilheit et al.*, 1991; *Berg and Chase*, 1992; *Petty*, 1994b; *Chiu et al.*, 1993].

The vertical distribution of latent heating depends on where the precipitation is formed, so we examine the relative partitioning of total precipitation water between the ice phase (IWP, ice water path) and the liquid phase (LWP, liquid water path) in cold precipitating systems. Because precipitation-sized ice particles can produce strong scattering at 85 GHz, the observed brightness temperature depression is directly related to IWP [*Adler et al.*, 1993; *Liu et al.*, 1994; *Petty*, 1994a, and references therein]. The LWP and IWP values, together with RR, determine the atmospheric vertical distribution of latent heating, which accounts for 30% of thermal energy that drives Earth's atmospheric circulation [*Chahine*, 1992]. Because precipitating cloud systems have very complicated vertical heating and cooling profiles, some studies [*Kummerow et al.*, 1989; *Kummerow and Giglio*, 1994a, b] have tried to estimate more details of the vertical profiles using SSM/I observations. However, it is very difficult to obtain a unique solution from observed data due to the limited number and frequencies of the SSM/I channels and the differences in their spatial resolutions.

This study combines the SSM/I and International Satellite Cloud Climatology Project (ISCCP) data sets, which are described in section 2. The microwave radiative transfer model simulations are discussed in section 3. On the basis of these simulations, a retrieval scheme for RR and the IWP and LWP of precipitation-sized particles for both cold and warm precipitating clouds is proposed and used to evaluate precipitating systems. Section 4 shows the results from 4 months of data over the global oceans (excluding polar regions). Section 5 summarizes our conclusions.

2. Data Sets

SSM/I radiances in the form of brightness temperatures are used in the microwave analysis. SSM/I measures polarized radiances at frequencies of 19.35, 22.235, 37.0, and 85.5 GHz (hereafter, 19, 22, 37, and 85 GHz). Both horizontal and vertical polarizations are measured at 19, 37, and 85 GHz, while only vertical polarization is measured at 22 GHz (these channels will be referred to as 19v, 19h, 22v, 37v, 37h, 85v, and 85h, respectively, and the corresponding brightness temperatures will be represented by Tb19v, Tb19h, Tb22v, Tb37v, Tb37h, Tb85v, and Tb85h, respectively). Spatial resolutions range from 70 x 45 km^2 at 19 GHz to 15 x 13 km^2 at 85 GHz. The microwave data are used to detect the presence of precipitation in clouds, to measure total water paths, and to infer precipitation rate. We separate water path into ice water path for precipitation-sized ice particles (ice particles in the cloud are too small to affect the microwave measurements) and total liquid water path (cloud plus precipitation). The choice of SSM/I analysis method is determined by whether cloud top temperature is above (warm cloud) or below freezing (cold cloud). Because of large uncertainties of microwave surface emissivity over land, we consider only maritime precipitating clouds.

The optical remote sensing data are from ISCCP [*Rossow and Schiffer*, 1991]. The ISCCP results we use are from the CX data set, which has information for individual satellite pixels (about 5 km in size) sampled at intervals of about 30 km and 3 hours as follows: satellite name, Earth location, surface type (land/water/coast), snow/ice presence, cloud/no-cloud decision, surface reflectivity and temperature, cloud optical thickness, and cloud top temperature/pressure. The ISCCP data, matched to SSM/I FOVs [*Lin and Rossow*, 1994], are used to detect clouds, to classify them as cold-topped or warm-topped, and to obtain sea surface temperatures (SST).

In this study, 4 months of SSM/I and ISCCP CX pixel level data from the first SSM/I annual cycle (August 1987, November 1987, February 1988, and May 1988) are collocated at pixel level covering 50°S–50°N latitude. A match between SSM/I and ISCCP observations requires time differences be ≤1.5 hours and separation distances between pixel centers be ≤30 km. In cases of multiple matches, the pixel pair with the minimum separation distance is used [*Lin and Rossow*, 1994]. The final monthly statistics are mapped at 2.5° spatial resolution.

3. Microwave Retrieval Method

3.1. Simulated Results

A plane-parallel microwave radiative transfer model is used to simulate the polarized radiances observed by SSM/I. This model is generally the same as used in many other microwave precipitation studies [e.g., *Wilheit et al.*, 1977; *Yeh et al.*, 1990; *Liu and Curry*, 1992; *Smith et al.*, 1992]. The atmospheric temperature and gas abundance profiles come from the tropical, midlatitude summer, and U.S. standard atmosphere (global mean) profiles [*McClatchey et al.*, 1972]. In our calculations, relative humidity is set to 100% within the cloud layers, while oxygen is assumed to be homogeneously mixed.

To account for the radiative effects of hydrometeors, a simplified vertical structure for precipitating cloud systems is assumed [cf. *Wilheit et al.*, 1977; *Wu and Weinman*, 1984; *Kummerow et al.*, 1989; *Liu and Curry*, 1992; *Petty*, 1994a]. Our hydrometeor profiles are the same as those of *Liu and Curry* [1992] except that we have two more standard cases (i.e.,

tropical and U.S. standard atmospheric profiles). The precipitating particle size distribution for both liquid and ice water is taken to be the *Marshall and Palmer* (M-P) [1948] distribution. The M-P distribution, used in many other studies, was originally derived for raindrops assumed to be spheres. Aircraft microwave observations [*Yeh et al.*, 1990] indicate good agreement for ice particle size distributions with the M-P distribution, especially in the upper portions of precipitation systems. We emphasize that the RR is implicit in the M-P distribution that gives the water content and size distribution of precipitation-sized particles: the size distribution times fall speed as functions of size gives RR. In our model, ice particles have a density of 0.7 g/cm^3, consistent with the range produced in model studies of particle growth [*Parrish and Heymsfield*, 1985], 0.5–0.8 g/cm^3. Also, a cloud layer with LWP = 25 mg/cm^2 and a constant layer thickness of 500 m below the freezing level is assumed to represent the non-precipitation-sized particles in precipitating clouds, following *Wilheit et al.* [1977, 1991]. Because the microwave radiances are insensitive to ice particles smaller than about 150 μm [cf. *Smith and Mugnai*, 1988, 1989; *Lin and Rossow*, 1994, and references therein], there is no ice cloud layer included in the model. The absorption, scattering, and extinction coefficients and phase functions are calculated according to Mie theory [e.g., *Tsang and Kong*, 1977]. The empirical formulae of *Ray* [1972] and tables of *Warren* [1984] are used to calculate the complex refractive indices of liquid and ice water droplets, respectively. *Liebe*'s [1985] model is used to determine atmospheric gas absorptions. Sea surface emissivity is calculated using *Petty*'s [1990] model with near-surface wind speed (WS) set to 7.5 m/s.

3.1.1. Cold-topped precipitating clouds. Because Tb22 is strongly affected by water vapor, we only consider the precipitation effects on Tb at the other three frequencies. The simulated relationships between SSM/I Tb and RR [cf. *Lin*, 1995] are very similar in shape to those of *Petty* [1994a] except Tb85 where our Tb decreases monotonically and near linearly with increasing RR. Comparing our Tb85 values with results based on a mesoscale convective cloud model [*Adler et al.*, 1991, 1993]: Tb85h = 251.0 - 4.19 RR, we find that our values are slightly higher. A key property of Tb19 and Tb37 is that they are strong, nonlinear (double-valued) functions of RR, which causes difficulties in their interpretation [*Wilheit et al.*, 1991; *Wu and Weinman*, 1984; *Chiu et al.*, 1990]. Although polarization differences can be used to choose a branch of the double-valued relationship (or to remove the double values), some ambiguity still exists because the nonlinearity depends on several properties of the precipitating system, as shown by warm precipitating cloud cases (see later discussion and also cf. *Petty* [1994a]). Because of the "cold" background of the ocean, Tb increases at first as RR (column opacity of water) increases from zero; however, when the amount of precipitation-sized ice at cloud tops becomes large enough at larger RR, ice scattering reduces Tb. Another factor that reduces Tb is the increasing emission height.

Since the FOVs of the lower frequency channels on SSM/I are larger (>30 km) than convective cells, radiances at these frequencies average over significant variations of RR. Some studies have found that the nonlinear dependence causes a significant underestimate of area-averaged RR (i.e., the beam-filling problem) by as much as a factor of 2 [cf. *Chiu et al.*, 1990; *Short and North*, 1990; *Liu and Curry*, 1992]. Using a very simplified three-dimensional (3-D) microwave radiative transfer model, *Petty* [1994a] found that this beam-filling problem may not be as quantitatively serious as suggested by other authors.

The higher sensitivity of Tb85 to scattering by large particles causes it to decrease monotonically with increasing RR (a secondary reason for the decrease is decreasing temperature of the emission level). Both simplified 3-D and more detailed modeling studies [*Petty*, 1994a; *Adler et al.*, 1991; *Smith et al.*, 1992; *Mugnai et al.*, 1993] show this same feature. For cloud systems with heavy rainfall (RR >10 mm/hr), Tb at all frequencies decreases because of increasing ice scattering opacity at cloud top [*Adler et al.*, 1991; *Smith et al.*, 1992; *Petty*, 1994a]. In fact, the scattering by precipitating ice particles is so strong that it can block the emission by the raindrop layer below. Thus, as *Mugnai et al.* [1993] showed in more detail, the microwave radiances are not sensitive to the liquid rainfall (or water content and size distribution) in the lowest portions of heavily precipitating clouds, which means that they cannot be used to estimate rainfall rates directly. Instead, microwave methods rely on an assumed relation between the magnitude of the ice effects and RR.

We can estimate the effects of changing emission level by subtracting the results with both ice and liquid hydrometeors from those of a liquid-only model (this is similar to warm precipitation as discussed below except warm cases have no hydrometeors above the freezing level). What remains is a near-linear relationship between the brightness temperature differences at 85 GHz and the ice water path of precipitation-sized ice particles up to IWP 600 mg/cm^2 (Figure 1; note that hereafter all Tb values represent the microwave radiances at the SSM/I viewing angle), since the effects of ice water particle size are secondary compared with ice water content (see next section). Note that ice scattering signals in Tb85 have been considered qualitatively in other studies [cf. *Petty*, 1994a; *Grody*, 1991; *Spencer et al.*, 1989]. The depression of Tb85 values represents ice water amount at the top of precipitating systems. When IWP > 1000 mg/cm^2, corresponding to a RR > 60 mm/hr, the nonlinear relationship between the difference and the IWP is strong, and it is difficult to retrieve the IWP. The lower part of Figure 1 also shows the relation between LWP and RR assumed in our retrieval scheme.

3.1.2. Warm-topped precipitating clouds. When the collocated ISCCP cloud top temperature is >0°C, the microwave Tb values are calculated without precipitating hydrometeors above the freezing level, as done by *Wilheit et al.* [1977, 1991]. Figure 2 shows the simulated Tb values; the lower right panel shows the difference Tb19v - Tb19h versus RR. Some differences occur for the different atmospheric profiles because the signal is dominated by emission which varies with the thickness of rainfall layer, atmospheric temperature and column water vapor (CWV). Because the Tb values are virtually constant at the higher frequencies for RR > 5 mm/hr, these radiances have little sensitivity to RR; hence a rainfall method based solely on Tb85, for example, is prone to miss warm, low RR cases. The last panel in Figure 2 shows that the polarization difference at 19 GHz is a more useful indicator of RR up to about 15 mm/hr. Colder atmospheric profiles exhibit larger differences for a given RR and saturate at higher RR because the colder atmosphere holds less rain water. Note that our polarization difference values are essentially the same as the normalized polarization differences used by *Petty* [1994a, b] except they are not normalized by the clear sky polarization difference (which does not depend on RR).

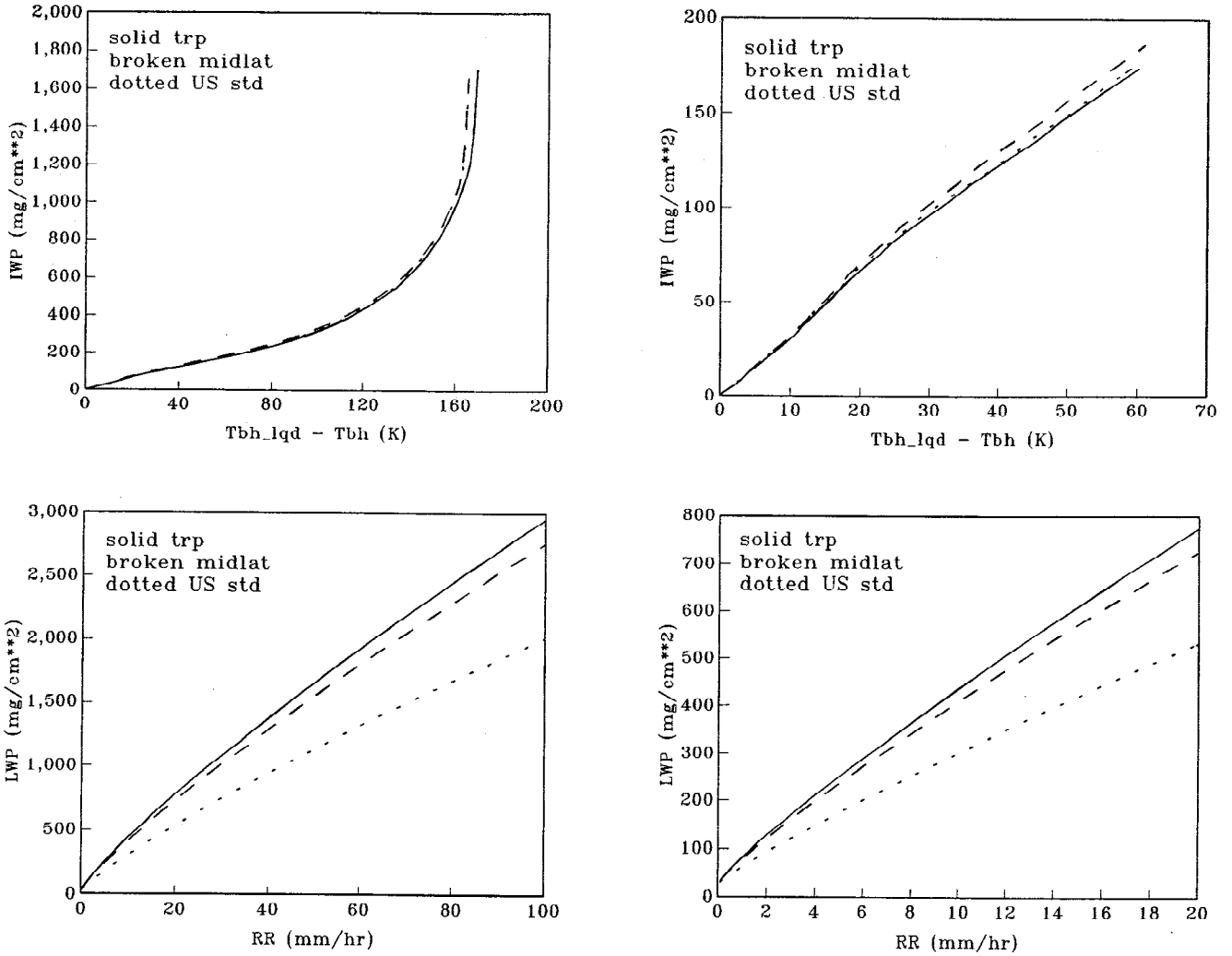

Figure 1. Ice water path ((IWP), upper panels) and liquid water path ((LWP), lower panels) retrieval scheme for tropical (solid curves), midlatitude summer (dashed curves), and U.S. standard atmosphere (dotted curves) profiles. Left panels give whole range of the method, while right panels exhibit the lowest end (near-linear parts). In this figure, Tbh_lqd - Tbh means the horizontally polarized brightness temperature (in kelvins) difference between liquid-only and full (ice and liquid) model.

The polarization difference at 19 GHz is still a nonlinear function of RR, especially when RR is larger than 10 mm/hr; hence variations of RR within the SSM/I FOV will cause an underestimate RR and LWP. Unlike cold-topped precipitation cases, there are almost no surface observations reported for warm-topped precipitation cases: in fact, there is generally no way to tell these two cases apart from surface observations except possibly with radar. Hence no estimates of beam-filling corrections for these systems have been made.

For our retrieval method, we compile the simulated relationships between Tb or Tb differences and RR, IWP, or LWP for the three atmospheric profiles into lookup tables and interpolate among them according to the ISCCP SST. If clouds are cold-topped, RR is estimated according to a table relating Tb85h and RR [*Lin*, 1995], which gives slightly larger RR values for the same Tb85h as assumed by *Adler et al.* [1991, 1993]; if the clouds are warm-topped, then a table relating Tb19v - Tb19h and RR or LWP is used (cf. Figure 2). The IWP values are obtained from the difference of Tb85h between a liquid-only model and the observed values (cf. Figure 1), while LWP is estimated from the retrieved value of RR (cf. Figure 1). We emphasize that the RR and LWP values are indirect retrievals and not calibrated against ground observations, although they are obtained using methods similar to others that have been compared. Thus there may be large biases in current RR estimates (see later discussion).

3.2. Sensitivity to Ice Particle Size

Because the scattering by precipitation-sized ice particles has such a strong effect on the 85 GHz signal and precipitating liquid water layer is often opaque at this frequency, other parameters, such as column water vapor (CWV), surface wind speed, and LWP for the nonprecipitating particles, have little effect [*Smith and Mugnai*, 1988; *Lin*, 1995]. Beam-filling effects have been considered by several authors [*Chiu et al.*, 1990; *Short and North*, 1990; *Adler et al.*, 1991; *Liu and Curry*, 1992; *Petty*, 1994a]. We do not reconsider the retrieval errors associated with these parameters. However, the model parameters, liquid and ice water content and precipitation size distribution, vary among the models used [cf. *Adler et al.*,

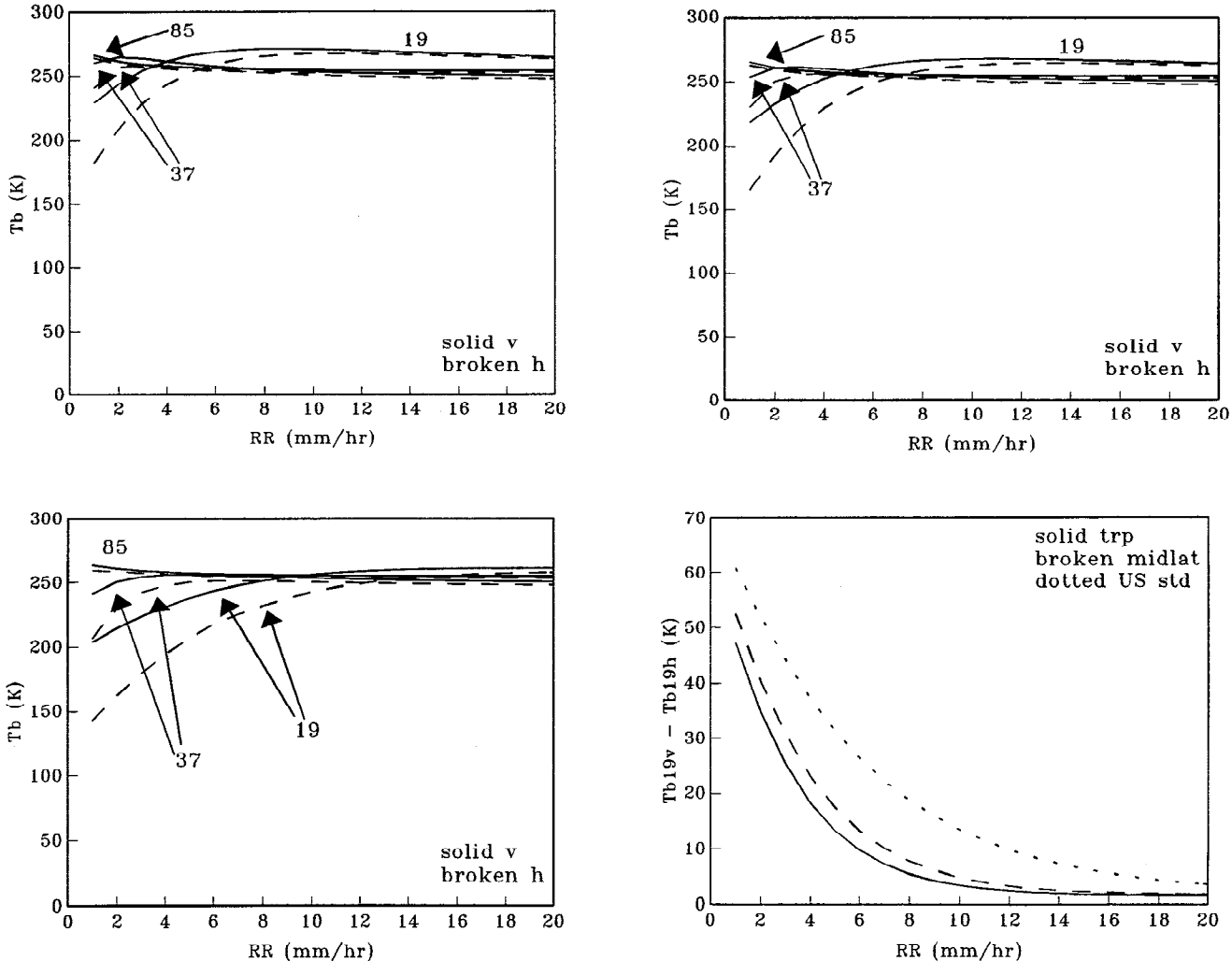

Figure 2. Simulated top-of-atmosphere Tb with vertical (solid curves) and horizontal (dashed curves) polarizations at 19, 37, and 85 GHz for warm-topped convective clouds for tropical (upper left panel), midlatitude summer (upper right panel), and U.S. standard atmosphere (lower panel) profiles. Lower right panel shows the values of Tb19v - Tb19h for tropical (solid curve), midlatitude summer (dashed curve), and U.S. standard atmosphere (dotted curve) profiles.

1991; *Smith et al.*, 1992; *Liu and Curry*, 1992; *Petty*, 1994a; *Kummerow and Giglio*, 1994a], and there are very few observations available for validation. Thus the same Tb values simulated by these models can correspond to different liquid and ice water contents. We investigate the sensitivity of our retrievals to the particle size distribution assumed in our radiative transfer calculations.

Figure 3 describes the variations of Tb85h in our model with different RR and IWP, referenced to the results for RR = 5 mm/hr. Negative differences indicate lower Tb85h values than for RR = 5 mm/hr. When IWP is held constant, variations in RR are linked to variations of liquid water content and particle size through the Marshall-Palmer distribution. Because changes in mean particle size are small for RR > 20 mm/hr [Lin, 1995], we only test RR = 10, 15, and 20 mm/hr cases. When IWP = 0 (i.e., liquid-only cases), increasing RR decreases Tb85h by about 4-8 K, but for clouds with only liquid hydrometeors, this change is caused almost entirely by the changing emission level assumed in the cloud model: at 85 GHz, the effect of increasing LWP has already saturated at RR = 5 mm/hr [*Lin*, 1995]. As IWP increases, Tb85h decreases even more dramatically (also cf. Figure 1 and *Lin* [1995]), but the differences of Tb85h between different RR models decrease by only 1-2 K (Figure 3) due to the differences in ice particle sizes. Hence liquid and ice particle size variations have little effect on the 85 GHz radiances compared with changes in ice water content (cf. Figures 1 and 3 [also see *Lin*, 1995]). This insensitivity to particle size means that the 85 GHz radiances are essentially directly proportional to IWP, which by assumption is proportional to both precipitation LWP and RR in our model and most others. The uncertainty in IWP corresponding to 1-2 K differences in Tb85 is about 3-5 mg/cm^2 (cf. Figure 1), about 15% of typical IWP values (see later discussion). This test demonstrates that IWP is the most directly observed quantity by SSM/I, while LWP and RR are dependent on the cloud and microwave radiative transfer models.

4. Analysis Results

The ISCCP data are more sensitive to the presence of the more numerous, optically thin, nonprecipitating clouds [cf. *Lin*

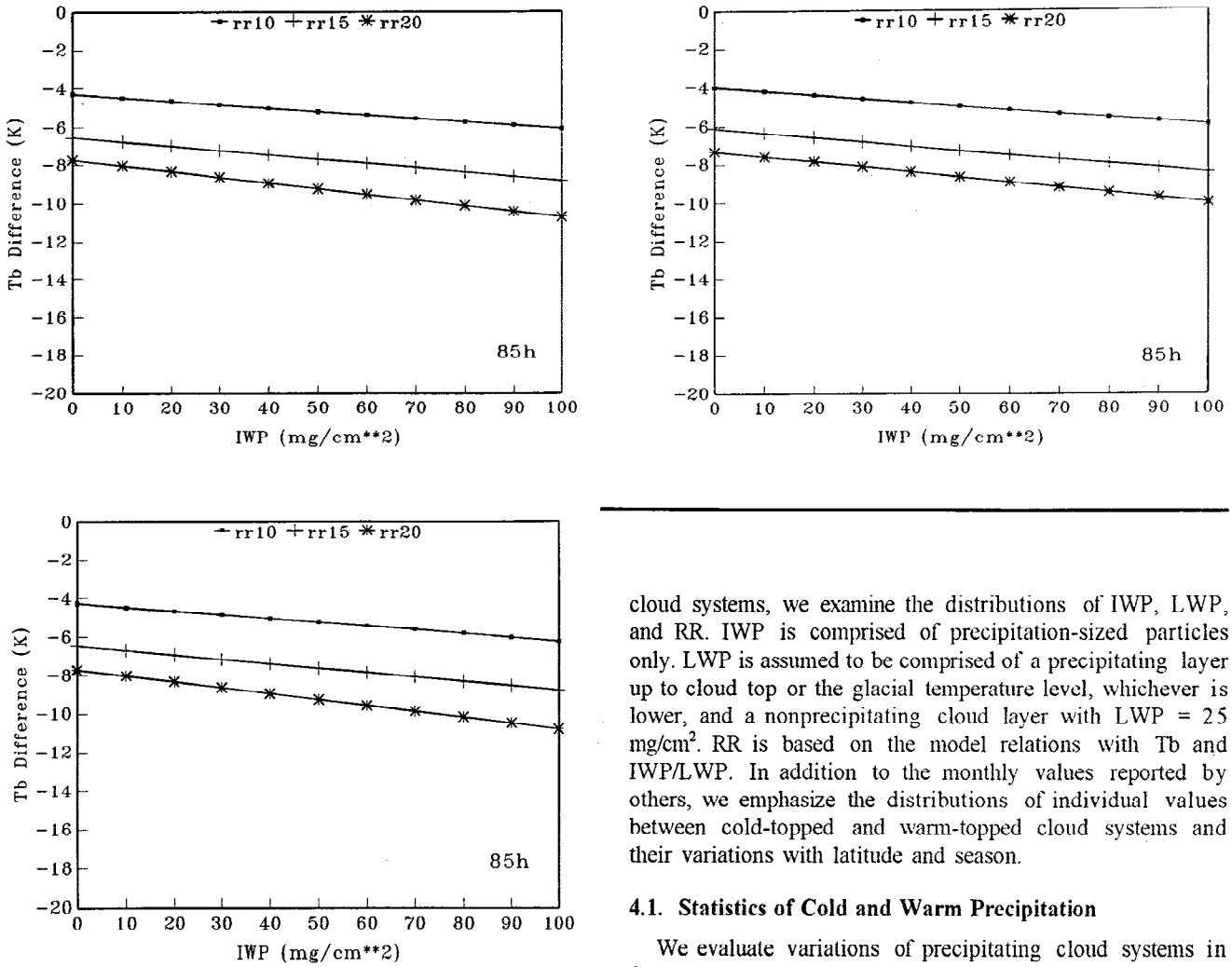

Figure 3. Sensitivity test for precipitation-sized hydrometeors for tropical (upper panels), midlatitude summer (upper right panels), and U.S. standard atmosphere (lower panels) profiles at 85 GHz. In this test, Tb values for rainfall rates (RR) = 5 mm/hr are used as a reference. Tb differences are calculated for RR = 10, 15, and 20 mm/hr, as indicated in the figure. Note that the Tb values at IWP = 0 (i.e., liquid-only cases) express the variations in emission level.

and Rossow, 1994] than the microwave measurements. Thus we use ISCCP data collocated with SSM/I to detect all clouds and to divide them into cold-topped (T ≤0°C) and warm-topped (T >0°C) clouds. The difference, Tb37v - Tb37h = 37 K, is used to separate nonprecipitating from precipitating systems [*Lin and Rossow*, 1994]. For cold-topped precipitating clouds, this criterion corresponds to a RR threshold in the range from about 0.3 mm/hr in the tropics to 0.5 mm/hr for the U.S. standard atmosphere, similar to values used by *Bauer and Schluessel* [1993] and *Kummerow and Giglio* [1994a]. For warm-topped precipitating clouds, this threshold corresponds to somewhat higher RR values from 0.5 mm/hr in the tropics to 0.9 mm/hr for the U.S. standard atmosphere.

Our threshold is also equivalent to the effect on microwave radiances of the presence of a cloud with LWP ≈ 50 mg/cm^2, similar to the value at which precipitation occurrence is about 50% [*Lin*, 1995]. Using these tests to isolate precipitating cloud systems, we examine the distributions of IWP, LWP, and RR. IWP is comprised of precipitation-sized particles only. LWP is assumed to be comprised of a precipitating layer up to cloud top or the glacial temperature level, whichever is lower, and a nonprecipitating cloud layer with LWP = 25 mg/cm^2. RR is based on the model relations with Tb and IWP/LWP. In addition to the monthly values reported by others, we emphasize the distributions of individual values between cold-topped and warm-topped cloud systems and their variations with latitude and season.

4.1. Statistics of Cold and Warm Precipitation

We evaluate variations of precipitating cloud systems in four geographic regimes: global (50°S–50°N), tropical (20°S–20°N), northern hemisphere midlatitudes (20°N–50°N), and southern hemisphere midlatitudes (20°S–50°S). Global Averaging (50°S–50°N), the frequency of precipitating systems, is about 5%: about 87% of them are cold-topped.

Figure 4 shows the frequencies of occurrence of IWP values for cold-topped precipitation clouds in the four regimes for August 1987, with the largest frequency normalized to unity (note that Figure 5 is similarly normalized). Table 1 gives the corresponding means and standard deviations for August and the other 3 months. Most cold-topped precipitating systems detected with our thresholds have IWP < 10 mg/cm^2, but a very few have IWP as much as 200 mg/cm^2. The global mean value of IWP for all cold-topped precipitating clouds is about 6-8 mg/cm^2 (Table 1); for "typical precipitation" systems, RR > 1 mm/hr (similar to Tb85h < 247 K cutoff used by *Adler et al.* [1993]), the mean IWP is about 27 mg/cm^2 (Table 2). The numerous very low IWP values reflect the fact that most of the precipitating systems detected are associated with light precipitation in which precipitation-sized ice particles represent considerably less water than the liquid droplets (see later discussion). Such values of IWP for precipitation-sized particles may be comparable with the IWP values for the smaller, nonprecipitating particles [cf. *Lin and Rossow*, 1996].

The LWP values for cold precipitating clouds (Table 1) are approximately 10 times larger than the IWP values with a mean value of approximately 80 mg/cm^2. This results from the fact that the liquid water layer is generally much deeper than the

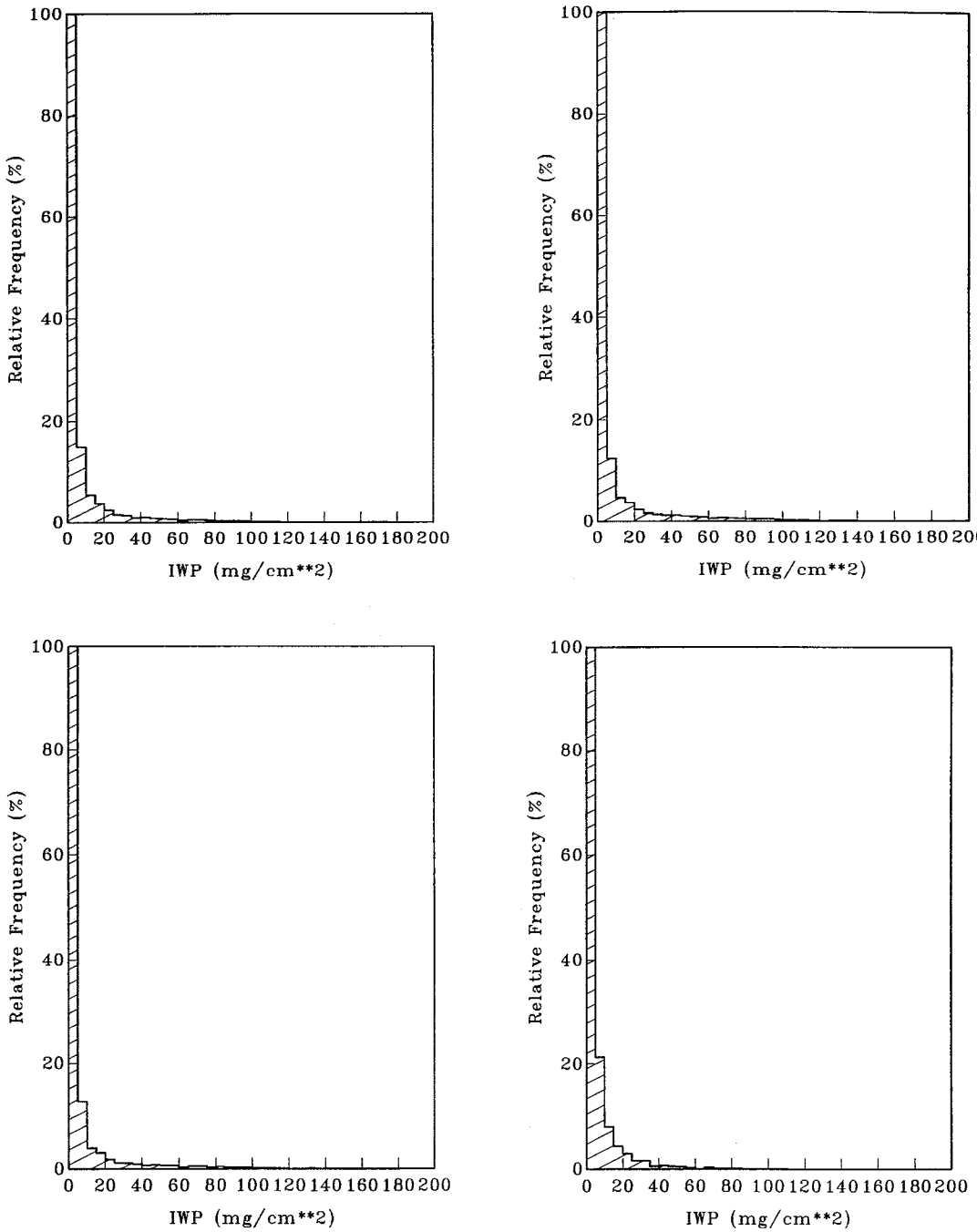

Figure 4. The frequencies of occurrence of IWP values for cold-topped precipitating clouds in August 1987, with the largest frequency normalized to unity. Here and Figure 5, the upper left, upper right, lower left, and lower right panels are the results for the global, tropical, northern midlatitude, and southern midlatitude geographic regimes, respectively.

ice water layer. Since in the tropics, the freezing level is much higher, LWP values are generally higher than at higher latitudes. If we eliminate systems with RR < 1 mm/hr, the average LWP values are several times larger, about 230 mg/cm^2 (Table 2). Extreme LWP values reach 1000 mg/cm^2. Such values of LWP for precipitating clouds were also found by *Liu and Curry* [1993]. Note that this scattering-based analysis method produces LWP values only slightly larger than our previous emission-based results as expected [cf. *Lin and Rossow*, 1994; *Lin*, 1995].

For all cold-topped precipitating clouds, the RR distributions have almost the same shape as the IWP distributions because of the model-assumed relationship between IWP and RR (or Tb85 and RR). Comparing our retrievals with those of *Adler et al.* [1993], we find that the shapes of the two distributions are the same, except our mean values (Table 3) are about 20% larger as expected [cf. *Lin*, 1995]. About 70–80% of cold-topped precipitating clouds have RR < 1 mm/hr, even with our detection threshold of about 0.3 mm/hr. RR > 20 mm/hr is extremely rare. The mean values of

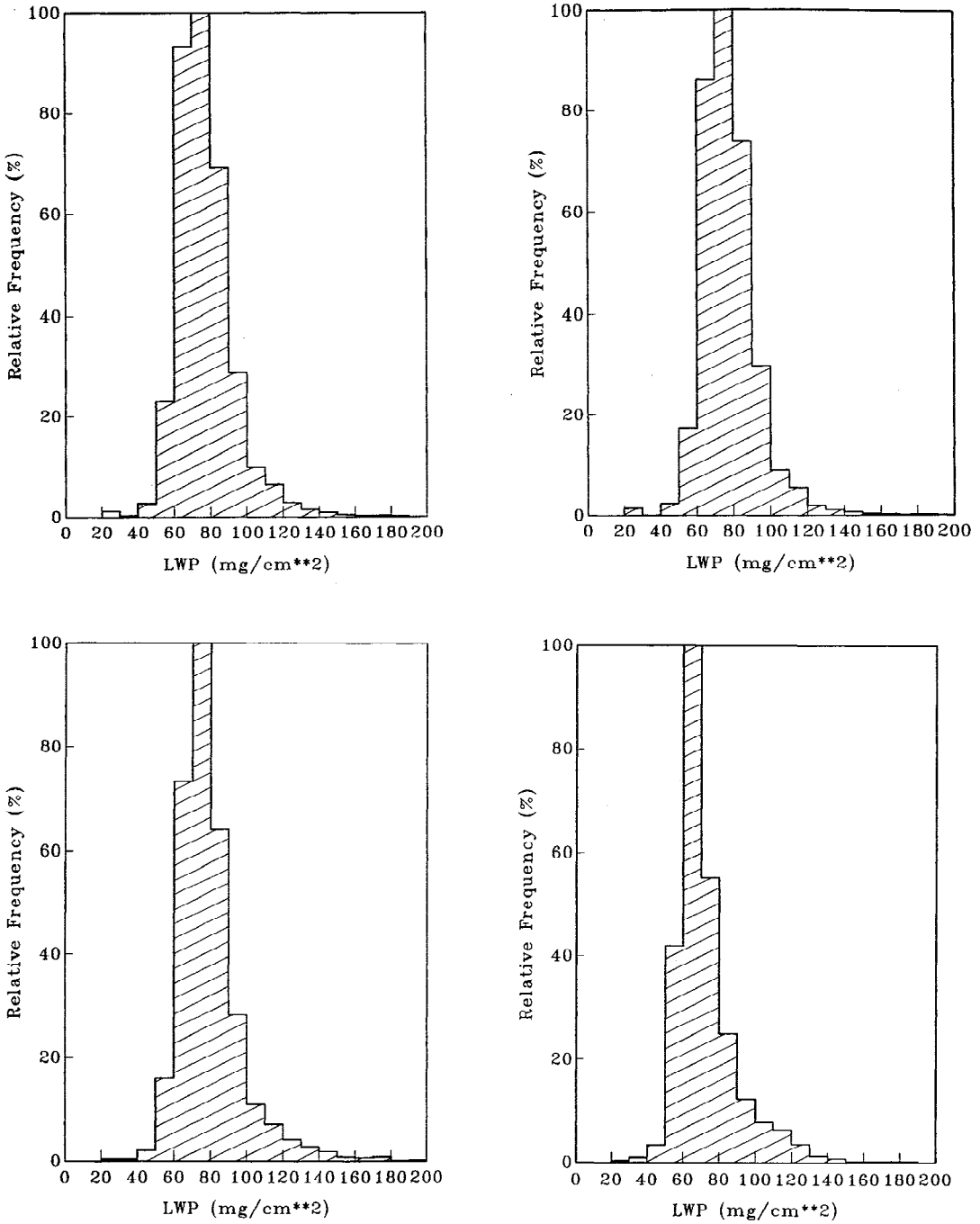

Figure 5. Same as in figure 4, but for the liquid water path (LWP) of warm-topped precipitating clouds.

RR is very small (about 1.5 mm/hr). RR in the tropics is generally higher than in midlatitude, and RR values in the northern hemisphere midlatitudes are higher than in the southern hemisphere. The standard deviations of estimated RR are about twice their mean values, indicating high variability of cold-topped rainfall systems (Table 3). Distributions like that shown in Figure 4 mean that collecting proper statistics is extremely challenging, since the monthly mean value can be influenced by one extreme, rare event in the distribution. This may mean that SSM/I-based precipitation statistics are not yet reliable because the sampling frequency of SSM/I is only about twice daily. The sampling rate problems have been considered in other studies [e.g., *Morrissy and Janowiak*, 1996; *Chang et al.*, 1993, and references therein].

Most of the precipitating systems are very near the limit of detection by SSM/I, which makes the average results sensitive to the detection thresholds used. For example, if we increase our threshold to RR = 1 mm/hr (not shown here [cf. *Lin*, 1995]), the mean RR is about 5.2 mm/hr (Table 3). The tropics and northern hemisphere midlatitudes have more systems with RR > 10 mm/hr than the southern midlatitudes. Although the mean value of RR is sensitive to the threshold, precipitation accumulations calculated with and without the lower RR values are similar to within about 20%: in other words,

Table 1. Mean and Standard Deviation of IWP and LWP for All Cold-Topped Precipitating Clouds

Global	Tropical	Northern Midlatitude	Southern Midlatitude.
		Aug. 1988	
8.24 ± 20.29	9.54 ± 22.54	7.19 ± 15.23	6.11 ± 14.62
88.82 ± 123.3	102.3 ± 141.4	83.48 ± 123.1	66.35 ± 74.26
		Nov. 1987	
7.42 ± 18.93	8.94 ± 21.20	7.11 ± 18.67	4.71 ± 13.57
82.68 ± 116.2	98.65 ± 136.1	75.80 ± 101.5	58.00 ± 76.17
		Feb. 1988	
6.88 ± 18.04	7.88 ± 20.74	7.61 ± 20.82	5.01 ± 14.58
77.05 ± 108.7	87.24 ± 126.3	71.34 ± 81.22	63.59 ± 88.41
		May 1988	
7.89 ± 19.55	9.37 ± 22.73	5.55 ± 16.01	7.24 ± 16.74
83.67 ± 116.5	98.53 ± 138.0	65.96 ± 94.88	74.16 ± 91.91

IWP, ice water path, upper lines; LWP, liquid water path, lower lines. Mean and standard deviation is in milligrams per cubic centimeters.

Table 3. Mean and Standard Deviation of RR for All and Typical (RR > 1 mm/hr) Cold-Topped Precipitating Clouds

Global	Tropical	Northern Midlatitude	Southern Midlatitude.
		Aug. 1987	
1.52 ± 3.26	1.74 ± 3.61	1.38 ± 3.22	1.22 ± 2.45
5.19 ± 4.64	6.07 ± 5.03	5.42 ± 4.94	3.70 ± 3.30
		Nov. 1987	
1.37 ± 3.07	1.65 ± 3.46	1.31 ± 2.90	0.90 ± 2.25
5.02 ± 4.54	5.89 ± 4.85	4.44 ± 4.26	3.73 ± 3.58
		Feb. 1988	
1.26 ± 2.93	1.41 ± 3.25	1.44 ± 2.76	0.93 ± 2.37
4.96 ± 4.43	5.72 ± 4.93	4.22 ± 3.46	4.26 ± 4.02
		May 1988	
1.45 ± 3.14	1.68 ± 3.56	1.04 ± 2.58	1.40 ± 2.80
4.95 ± 4.46	5.96 ± 4.97	4.37 ± 4.11	4.10 ± 3.72

Mean and standard deviation is in millimeters per hour. All cold-topped precipitating clouds, upper lines; typical, lower lines.

although the cloud systems with RR < 1 mm/hr are the most common and cover the most area, they contribute only about 20% to the total precipitation. This fact also means that rare, large events are important to the precipitation total, exaggerating the sampling problem [also see *Wilheit et al.*, 1991; *Chang et al.*, 1993].

We do not find extremely heavy precipitation systems with RR > 60 mm/hr; our maximum value of RR for this 1 year is about 42 mm/hr during February 1988. *Jones and Sims* [1978] report larger RR values, but their statistics cover both land and ocean, while ours cover only oceans. *Adler et al.* [1993] also find that the heaviest rainfall occurs over land.

Seasonal variations of mean RR in the large geographic domains are small (Table 3). The phase of the global mean annual cycle follows that of the tropics where the rainfall rates are both largest and most frequent. Averaging over ± 20° latitude for the tropical zone mitigates the effects of the strong latitudinal shifts in precipitation that occur with season (see next section). In midlatitudes, more precipitation is produced in the colder seasons (even though we neglect the contribution of snowfall [see *Liu and Curry*, 1996]).

Figure 5 shows the distribution of LWP for warm-topped precipitating clouds (ISCCP cloud top temperature > 0°C) for August 1987. These histograms are symmetrical about their mean values because the precipitation detection threshold eliminates smaller values (nonprecipitating clouds) and the upper limit on the depth of the layer below the freezing level sets a rough upper limit on LWP. The mean LWP value of warm-topped precipitating clouds is approximately 75 mg/cm^2 (Table 4), slightly lower than for cold-topped precipitating clouds. If the differences in RR detection thresholds for cold-topped and warm-topped precipitating clouds were removed, then cold-topped precipitating clouds would be found to hold more liquid water than warm-topped precipitating clouds as expected. These LWP estimates are very similar to our previous emission-based estimates [*Lin*, 1995; *Lin and Rossow*, 1994] since the scattering at 19 GHz is weak.

In the distribution of RR for warm-topped precipitating clouds [cf. *Lin*, 1995], the peak frequency does not occur at the smallest RR values because the detection threshold we use eliminates values <0.5–0.9 mm/hr, depending on the atmospheric profile. There are almost no warm precipitation

Table 2. Mean and Standard Deviation of IWP and LWP for Typical (RR > 1 mm/hr) Cold-Topped Precipitating Clouds

Global	Tropical	Northern Midlatitude	Southern Midlatitude.
		Aug. 1987	
27.84 ± 32.13	33.19 ± 35.11	29.85 ± 35.56	18.40 ± 22.09
231.1 ± 171.3	281.3 ± 184.7	243.2 ± 181.5	145.7 ± 94.41
		Nov. 1987	
26.92 ± 31.04	31.79 ± 33.30	23.94 ± 30.36	19.27 ± 23.86
225.3 ± 166.7	274.9 ± 179.0	188.3 ± 144.8	155.6 ± 118.4
		Feb. 1988	
26.71 ± 30.50	31.78 ± 35.16	20.93 ± 20.89	22.69 ± 27.22
218.2 ± 159.6	264.0 ± 178.9	157.4 ± 96.31	191.2 ± 144.2
		May 1988	
26.69 ± 30.88	33.10 ± 35.59	23.22 ± 28.25	21.09 ± 24.49
261.2 ± 161.8	273.8 ± 180.6	189.3 ± 148.9	164.6 ± 119.8

RR, rainfall rate. Mean and standard deviation is in milligrams per cubic centimeters.

Table 4. Mean and Standard Deviation of RR and LWP for Warm-Topped Precipitating Clouds

Global	Tropical	Northern Midlatitude	Southern Midlatitude.
		Aug. 1987	
1.48 ± 0.67	1.39 ± 0.52	1.65 ± 0.93	1.76 ± 0.87
77.05 ± 16.46	77.39 ± 15.28	79.63 ± 19.01	72.93 ± 18.02
		Nov. 1987	
1.59 ± 0.74	1.47 ± 0.49	1.63 ± 1.04	2.15 ± 0.96
78.86 ± 17.19	79.69 ± 14.36	78.69 ± 24.08	76.14 ± 17.61
		Feb. 1988	
1.55 ± 0.61	1.51 ± 0.53	1.45 ± 0.82	1.75 ± 0.68
77.78 ± 15.00	79.38 ± 14.50	69.34 ± 15.09	77.98 ± 14.94
		May 1988	
1.66 ± 0.84	1.59 ± 0.83	1.86 ± 0.82	1.88 ± 0.88
80.65 ± 20.44	82.00 ± 21.24	78.81 ± 15.49	74.94 ± 17.89

Mean and standard deviation is in millimeters per hour and milligrams per cubic centimeters, respectively. RR, upper lines; LWP, lower lines.

rates >8 mm/hr because warm-topped precipitating clouds, by definition, occupy shallower layers than cold-topped systems. This result is also exaggerated somewhat by the large 19 GHz SSM/I FOV that reduces the magnitude of RR by averaging over an area larger than the precipitation system.

The mean RR value for warm-topped precipitating clouds is approximately 1.5 mm/hr (Table 4), roughly the same as for cold-topped precipitating clouds. In the tropics, the mean RR for warm-topped precipitating clouds is lower than for cold-topped precipitating clouds, despite a higher RR detection threshold (Tables 3 and 4), indicating that warm-topped precipitating clouds produce less precipitation than cold-topped precipitating clouds. In midlatitudes, the mean RR value for warm-topped clouds is similar to RR for cold-topped clouds. Although larger RR values are more frequent in cold-topped precipitating clouds than in warm-topped clouds, this difference is smaller in midlatitudes. The standard deviations of RR for warm-topped precipitating clouds (Table 4) are approximately half of their mean values (about 0.7 mm/hr), suggesting that variations of warm precipitation are small at ≈40 km scale.

4.2. Comparison of Estimated RR Values With Surface Observations

There are very few observations available of the properties of precipitating systems over open oceans, as mentioned in the introduction, especially of IWP and LWP. The only reliable RR surface measurements are daily precipitation reports from rain gauges on small tropical atolls [*Morrissey et al.*, 1995] (hereafter referred as Atoll), which have been used to validate other precipitation analyses [*Spencer*, 1993; *Adler et al.*, 1994; *Barrett et al.*, 1994, and references therein]. The sparse sampling of SSM/I will affect this comparison, so long time records (probably more than a month) are required to obtain accurate mean values. On the other hand, the Atoll data may poorly represent the rainfall over a 2.5° grid box since few grid boxes have more than one Atoll station. Thus we compare the average RR values from all 4 months in 2.5° grid boxes with the Atoll sites, which gives 38 data points. In the Precipitation Intercomparison Project-1 (PIP-1) only the 2.5° grid boxes that contained at least three atoll stations were used for 4 monthly means [*Barrett et al.*, 1994], which yielded about 28 data points. The PIP-1 studies found that there were large differences among all precipitation estimates ranging from underestimates by a factor of about 2 to overestimates by a factor of 2: more satellite algorithms seemed to produce underestimates than overestimates. Figure 6 shows the scatterplot of our SSM/I determinations of RR versus the Atoll measurements (note change of units to millimeters per day). One striking feature is that our RR values are near linearly related to the Atoll data with a high correlation (= 0.84), which demonstrates the ability of SSM/I to monitor rainfall variations. This result was also found in PIP-1. Quantitatively, our SSM/I estimates are about 1/4 lower than of Atoll with a mean bias of about 1.8 mm/d and RMS errors (after bias removed) of 2.2 mm/d. The underestimate by our method is not a surprise. Comparing their rainfall estimates with the Atoll data, *Adler et al.* [1994] found a factor of 2 underestimate, so they increased their rainfall estimates by factor of 2 empirically. Our retrievals are about 20% larger than those of *Adler et al.* [1993] for cold precipitating clouds with the same Tb85 value and include both cold-topped light

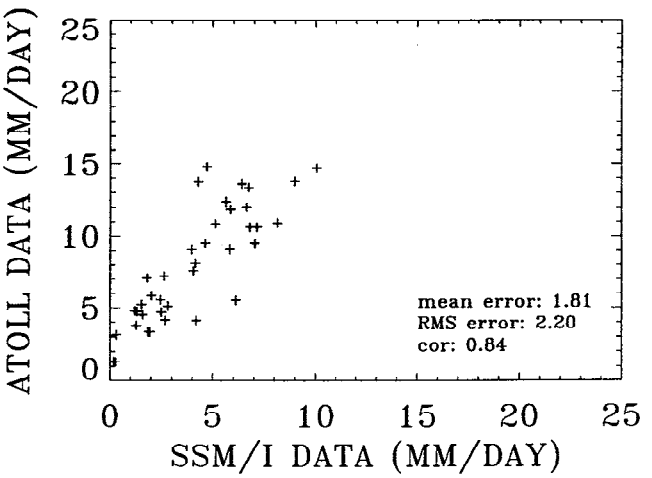

Figure 6. Scatterplot of the comparison between SSM/I-based rainfall rates and Atoll observations for 4-month averages. The bias and RMS errors (after bias removed) and the correlation coefficient are indicated in the figure.

precipitation (RR< 1 mm/hr) and warm-topped precipitation; the latter two increase RR by another 20 and 10%, respectively. Hence our underestimate of RR is significantly less than 2. With the limited validation data available, we cannot say how large the bias in our retrievals is (although it is probably less than a factor of 2). Nevertheless, our RR values appear to capture the variations of precipitation over oceans, as most satellite algorithms do [*Barrett et al.*, 1994; *Janowiak et al.*, 1995]. More validation may become available from the Tropical Rainfall Measuring Mission.

4.3. Near-Global Distribution of Total Precipitation

Monthly, zonal mean RR values for the 4 months are shown in Figure 7 (solid lines). Significantly higher precipitation rates appear in the tropics compared with midlatitudes: peak RRs are as high as about 7 mm/d, whereas values in midlatitudes are about 1–2 mm/d, occasionally 3 mm/d. The high RR zone, the Intertropical Convergence Zone (ITCZ), remains in the northern hemisphere in all 4 months. In the northern hemisphere, the cold seasons have higher precipitation rates and larger latitudinal gradients of RR than the warm seasons, with a local minimum of approximately 0.2–0.3 mm/d in the subtropics and a maximum of about 3 mm/d in the midlatitude cyclone zone. In the southern hemisphere, precipitation rate contrasts between cold and warm seasons are small, but the maximum of about 2 mm/day shifts from 10°–20°S in the summer to 30°–40°S in winter. During the transition seasons, the precipitation is nearly uniform with latitude at about 1 mm/d. The dashed lines in Figure 7 show the contribution to the total precipitation rate made by cold-topped precipitating clouds, indicating that they dominate the total precipitation due to their higher frequencies than of warm precipitating systems, though the contribution of warm-topped systems is slightly larger in the warm season. The largest contribution of warm-topped precipitating clouds occurs in the tropics, where the thickness of the surface to freezing-level layer is the largest. In the colder midlatitudes, the thickness of this layer is small, so significant warm precipitation is rare. Since there are no global surface RR observations available over oceans, we can quantify our errors.

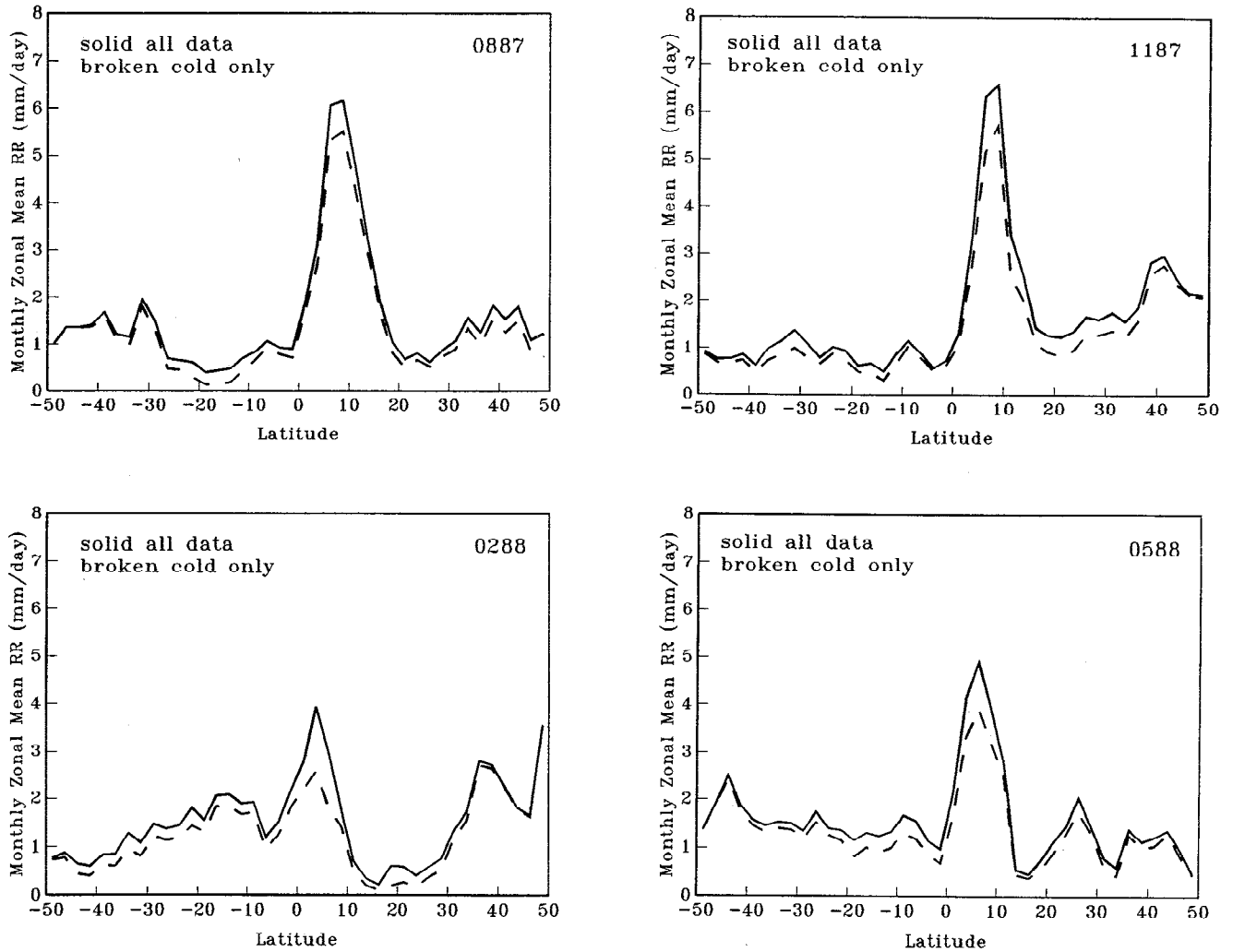

Figure 7. Monthly, zonal mean rainfall rates in millimeters per day for August 1987 (upper left), November 1987 (upper right), February 1988 (lower left), and May 1988 (lower right). Solid curves are the estimates for of all precipitating clouds, while dashed ones are the estimates for cold-topped precipitating clouds.

Compared with the 18 precipitation estimates in PIP-1, our current results underestimate monthly precipitation.

Figure 8 shows the geographic distribution of the monthly mean frequency of occurrence of cold-topped and warm-topped precipitating clouds for February 1988 (other months are similar [cf. *Lin*, 1995]). Frequency is calculated as the ratio of the number of precipitating SSM/I pixels to all available pixels (even clear ones) in each grid box. Precipitating clouds occur very infrequently in general: peak frequencies for cold-topped precipitating clouds are about 15% in tropics and about 10% in midlatitudes, while for warm-topped precipitating clouds, they are about 2%. Peak frequencies occur in the ITCZ, the South Pacific Convergence Zone (SPCZ), and in the midlatitude storm tracks. In the tropics, there appears to be relatively more cold-topped precipitation in the warmer regions of the tropical oceans and relatively more warm-topped precipitation in the cooler regions.

Averaging over all oceans between 50°S and 50°N, the frequency of occurrence of precipitation is about 5%, which is much lower than inferred from ship observations [*Petty*, 1995]. Beside missing snowfall in the microwave analysis, there are two obvious reasons that can produce this difference: (1) our fixed rainfall detection thresholds will cause us to miss more light precipitation in the extratropics than in the tropics, and (2) our current method does not detect very light rainfall (RR < 0.3 mm/hr) and/or drizzle at all (see later discussion). It seems that state-of-art satellite rainfall techniques basically detect fewer precipitation systems than ship observations [*Petty*, 1995]. Relatively heavy precipitation (RR > 5 mm/hr) occurs almost exclusively in cold-topped cloud systems (at a spatial scale ≈ 40 km) with a frequency of only about 0.5%, really heavy precipitation (RR > 10 mm/hr) occurs < 0.2% of the time. However, the precipitation accumulations of the systems with RR > 5 mm/hr and RR > 10 mm/hr are about 50 and 30% of the total, respectively. These results imply that the very rare, heavy precipitation systems are very important to precipitation totals, so that high sampling rates are extremely critical for accurate results.

Although cold-topped precipitation dominates in the tropics, as expected, warm precipitation is generally 10–20% of the total (Figures 7 and 8). While cold-topped precipitating clouds in the western Pacific shift from the northern

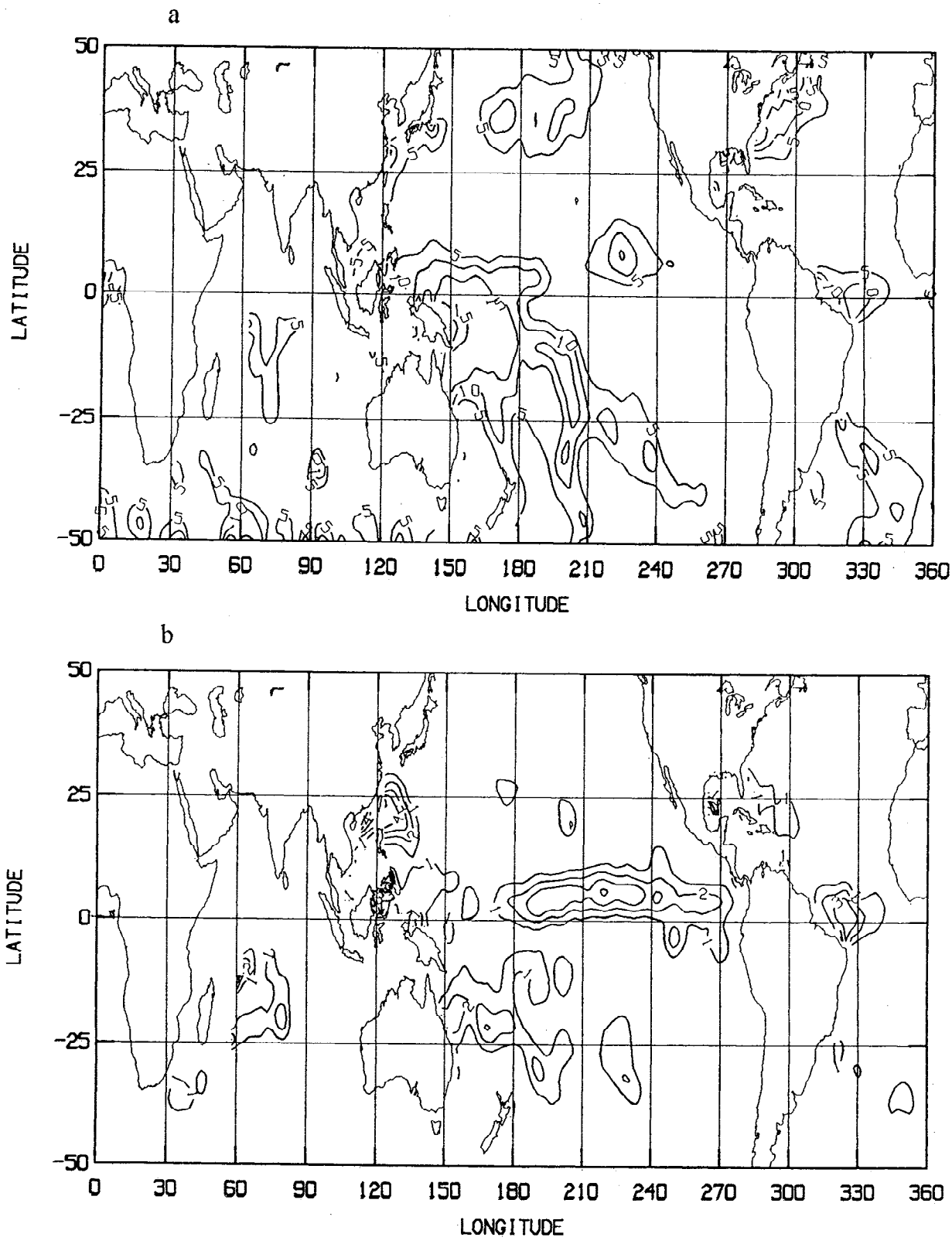

Figure 8. Monthly mean frequencies of occurrence of (a) cold-topped and (b) warm-topped precipitation for February 1988.

hemisphere in boreal summer to the southern hemisphere in boreal winter, cold-topped precipitating clouds in the eastern Pacific remain in the northern hemisphere but move from a more northerly to a more southerly position. When the cold-precipitating clouds move away, they are replaced by significant amounts of warm-topped precipitating clouds, especially in the central Pacific, which can contribute as much as one third of the total precipitation locally (Figures 7 and 8

for February 1988). During northern hemisphere winter, the active interactions between tropical plumes and midlatitude cyclone systems [*Janowiak et al.*, 1995; *McGuirk et al.*, 1988] may produce more shallow convective clouds than during summer seasons, contribute significant amounts of precipitation to the monthly rainfall totals, and maintain local maxima for the whole annual cycle [cf. *Janowiak et al.*, 1995] (also see later discussion). Thus, warm precipitation cannot be neglected especially in the tropics.

Plate 1 shows the geographic distribution of monthly mean RR (in units of millimeters per day) for the 4 months. During August (upper left), the ITCZ is associated with a peak concentration of heavy precipitation located at about 10°N. The SPCZ is well-developed and clearly separate from the ITCZ. The tropical western Pacific warm pool is at its warmest stage, and mean precipitation rates are as high as 14 mm/d. In the tropical eastern Pacific and the tropical Atlantic, heavy precipitation (about 10 mm/d) occurs in some locations. In midlatitudes, moderate to heavy precipitation (about 6 mm/d) occurs in the storm tracks, primarily in the cyclogenesis regions off the east coasts of the continents, particularly South America. Only very weak, warm precipitation (<1 mm/d) occurs in the regions of mean subsidence and persistent marine stratocumulus clouds. During February (lower left), the ITCZ shifts southward, and the SPCZ becomes more extensive. Compared with August, precipitation in northern midlatitudes over the Pacific shifts downstream into the central Pacific. The storm track precipitation in the midlatitude South Atlantic weakens from August to February while strengthening in the northern Pacific. The Indian Monsoon is a notable feature in May 1988 (our statistics in this area are poor because of the lack of geostationary satellite, INSAT, data in ISCCP). Heavy precipitation occurs along the coast of the Indian subcontinent and in the central Indian Ocean.

Plate 2 is a map of annual precipitation totals. The peak value (about 5000 mm) is located in the eastern Pacific [cf. *Spencer*, 1993; *Janowiak et al.*, 1995] due to persistent heavy precipitation during the whole year (cf. Figure 9). Although precipitation is concentrated near islands in the western Pacific during boreal summer, the concentration shifts to other locations in other seasons. Consequently, the persistent precipitation located to the east of the maritime continent dominates the annual accumulation (approximately 5°N, 150°E). The Indian Ocean and SPCZ also have large accumulations. Moderate accumulations occur in the midlatitude storm track with concentrations in and near the

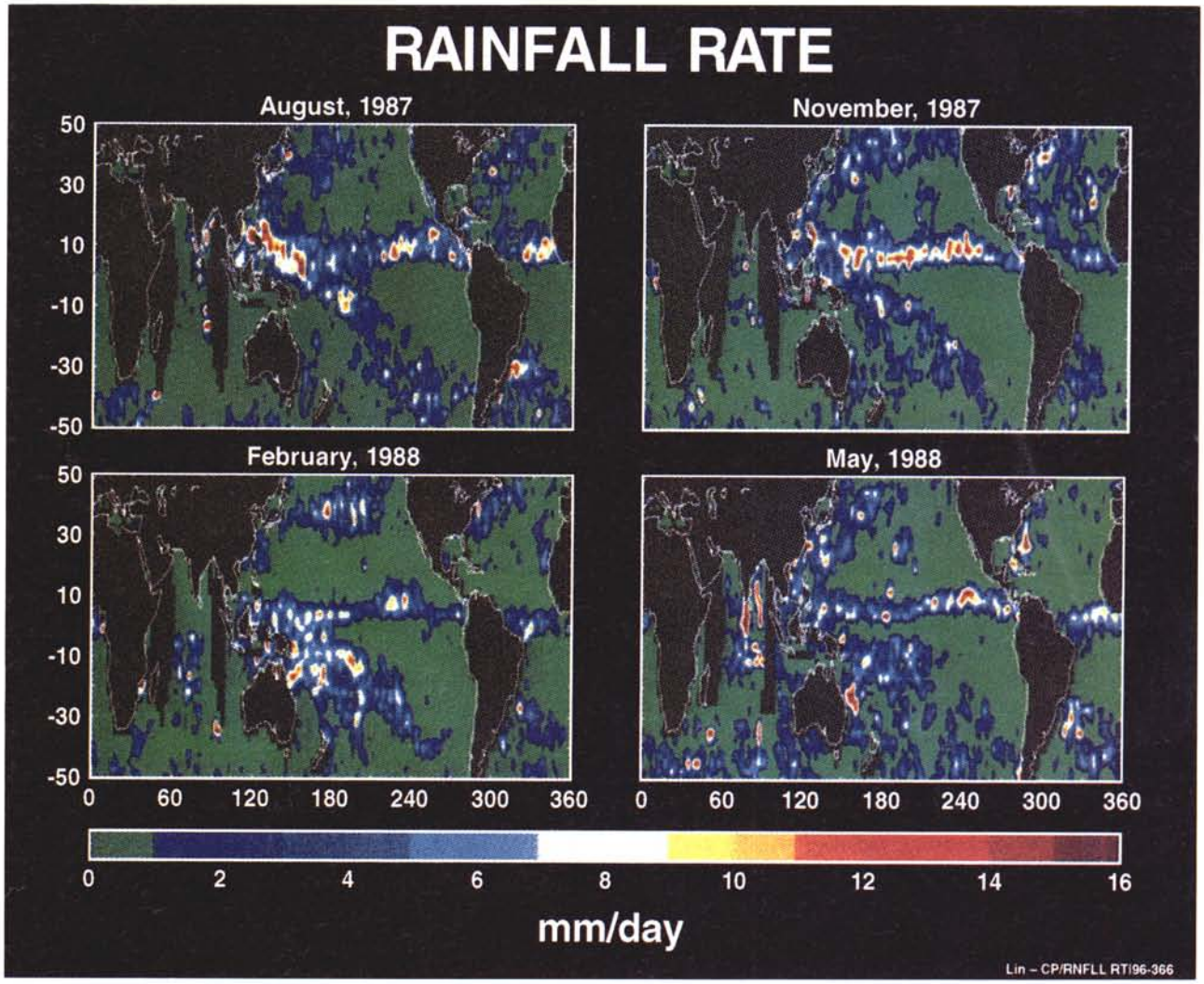

Plate 1. Monthly mean precipitation in millimeters per day for August 1987, November 1987, February 1988, and May 1988.

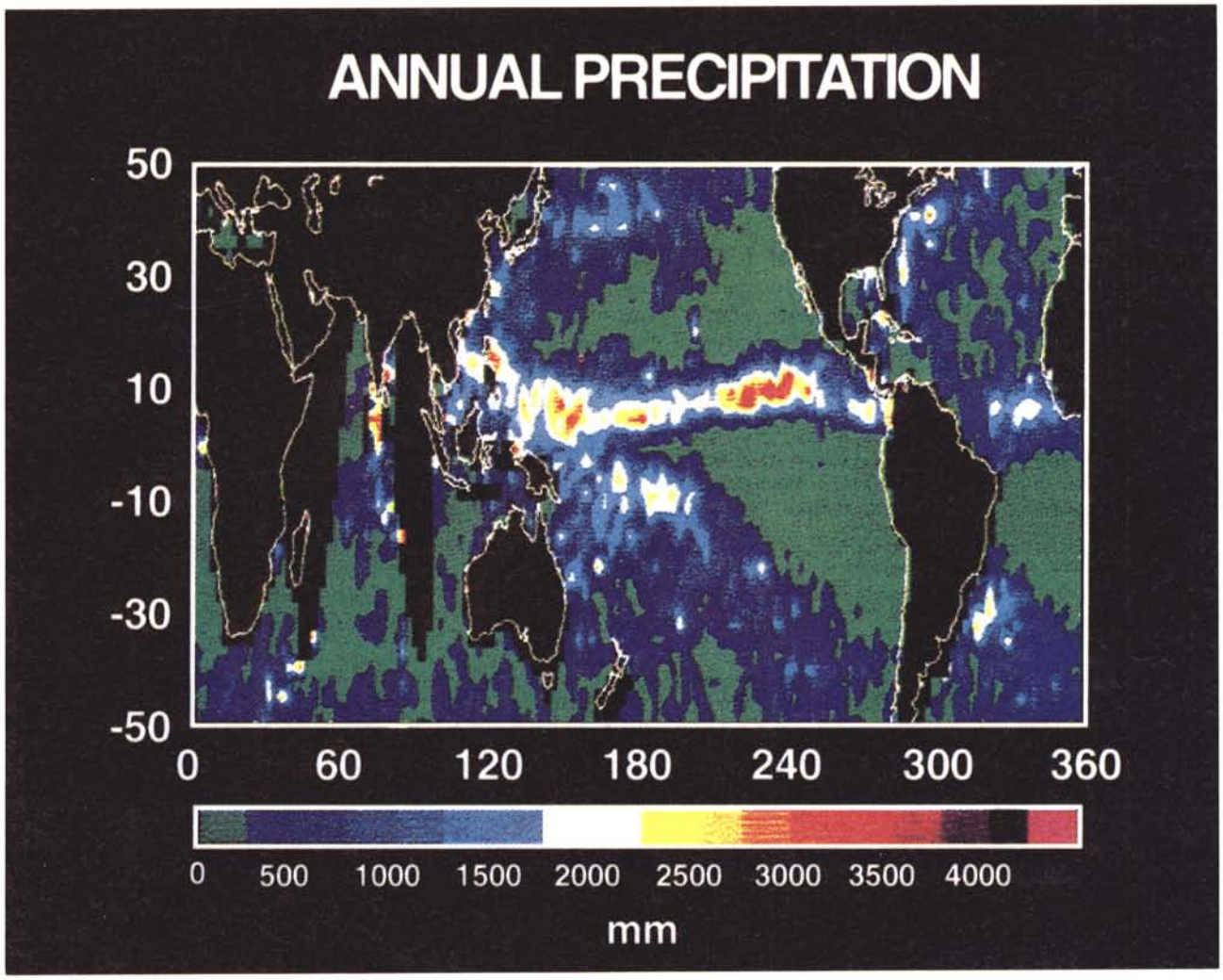

Plate 2. Annual total precipitation in millimeters based on 4-months observations.

continental east coast cyclogenesis regions. Some recent observations indicate that persistent drizzle may be common in the marine stratocumulus regimes, for example, during the First ISCCP Regional Experiment (FIRE) [*Paluch and Lenschow*, 1991; *Minnis et al.*, 1992]. Because the drizzle drops are relatively small compared with other forms of precipitation [*Paluch and Lenschow*, 1991] and LWP for these clouds is generally <25 mg/cm^2 with an average of ≈10 mg/cm^2 [*Blaskovic et al.*, 1991; *Lin*, 1995; *Lin and Rossow*, 1994], the microwave effects of these clouds and their drizzle are very weak. Thus SSM/I probably misses some or all of this form of precipitation.

5. Summary

On the basis of a microwave radiative transfer model, this study combines SSM/I and ISCCP data to estimate IWP, LWP, and RR values for precipitating systems. The advantage of using ISCCP data is that deep convective or anvil precipitating clouds can be separated from shallow convection so that scattering-based or emission-based algorithms can be selected automatically. We found that a separation of ice-containing and ice-free precipitating systems helps reduce the tendency of microwave technique to underestimate RR and that improving the detection of low-RR systems is also important to reducing this tendency.

This study made the first near-global investigation on IWP and LWP values for precipitation systems and found that IWP values for precipitation-sized particles are quite variable. Some clouds hold as much as 200 mg/cm^2 of precipitation ice water, while others have as little as 5 mg/cm^2. The mean value is small (about 7 mg/cm^2) for all cold-topped precipitating clouds, while the value for typical (RR > 1 mm/hr) cold-topped precipitating clouds is approximately 3 times larger (about 27 mg/cm^2). The mean LWP value for cold-topped precipitating clouds is rather large, approximately 80 and 230 mg/cm^2 for all and typical cold precipitating clouds, respectively. Occasionally, LWP reaches very high values of 500–1000 mg/cm^2. The large variations and extreme values in IWP and LWP for cold-topped precipitating clouds indicate that cold precipitation is extremely variable spatially and temporally.

The RR estimates from microwave measurements are basically indirect measurements, which require surface observational data to calibrate the retrieval algorithm. The global mean values for cold-topped precipitating systems are about 1.5 m/hr, and their variations are large.

The estimated LWP and RR values for warm-topped precipitating clouds are generally near the average value because they are estimated from Tb19, which has a large (40+ km) FOV. Generally, rainfall systems averaged over this spatial scale appear weak. The mean value of RR is similar to cold-topped precipitating cases. Because the RR detection threshold for warm precipitating clouds is higher than for cold cases, there are probably many more warm precipitation systems with very low RR values. The mean LWP value is approximately 75 mg/cm^2, which is slightly lower than cold-topped precipitating clouds due to shallower rain water layers.

The geographic distribution of warm-topped precipitating clouds is not the same as for cold-topped precipitating clouds. Cold-topped precipitating clouds usually exist in warm SST regions, while warm-topped precipitating clouds occur in slightly cooler regions. This may occur because organized deep convection may inhibit development of shallow, warm precipitating clouds. Generally, total precipitation is dominated by the cold-topped precipitating systems, but warm precipitation contributes about 10–20% of the total. Sometimes (e.g., February 1988) warm-topped precipitation contributes a larger portion (about 1/3) of the total in the tropics. These results illustrate that warm precipitation is not negligible.

In addition to biases produced by the microwave algorithm, SSM/I-based results may be biased by poor sampling of diurnal variations: the present estimates only represent the average of early morning and later afternoon observations. The Tropical Rainfall Measuring Mission [*Simpson et al.*, 1988] should provide better understanding of this sampling problem.

Acknowledgments. The authors would like to express our appreciation to R. Adler, A. Del Genio, D. Rind, and B. Wielicki for their helpful comments. This study is supported by NASA Global Radiation Data and Modeling Program. One of us (B.L.) also acknowledges the support from NASA Cloud and the Earth's Radiant Energy System under contract NAS1-19656.

References

Adler, R.F., H.-Y. Yeh, N. Prasad, W.-K. Tao, and J. Simpson, Microwave simulations of tropical rainfall system with a three-dimensional cloud model, *J. Appl. Meteorol., 30*, 924-953, 1991.

Adler, R.F., A.J. Negri, P.R. Keehn, and I.M. Hakkarinen, Estimation of monthly rainfall over Japan and surrounding waters from a combination of low-orbit microwave and geosynchronous IR data, *J. Appl. Meteorol., 32*, 335-356, 1993.

Adler R.F., G.F. Huffman, and P.R. Keehn, Global tropical rain estimates from microwave-adjusted geosynchronous IR data, *Remote Sensing Rev., 11*, 125-152, 1994.

Barrett, E.C., et al., The first WetNet precipitation intercomparison project (PIP-1): Interpretation of results, *Remote Sen. Rev., 11*, 303-373, 1994.

Bauer, P., and P. Schluessel, Rainfall, total water, ice water, and water vapor over sea from polarized microwave simulations and special sensor microwave/imager data, *J. Geophys. Res., 98*, 20737-20759, 1993.

Berg, W., and R. Chase, Determination of mean rainfall from the special sensor microwave/imager (SSM/I) using a mixed lognormal distribution, *J. Atmos. Oceanic Technol., 9*, 129-141, 1992.

Blaskovic, M., R. Davies, and J.B. Snider, Diurnal variation of marine stratocumulus over San Nicolas island during July 1987, *Mon. Weather Rev., 119*, 1469-1478, 1991.

Broecker, W.S., Unpleasant surprises in the greenhouse?, *Nature, 328*, 123-126, 1987.

Chahine, M.T., The hydrological cycle and its influence on climate, *Nature, 359*, 373-380, 1992.

Chang, A.T.C., L.S. Chiu, and T.T. Wilheit, Random errors of oceanic monthly rainfall derived from SSM/I using probability distribution functions, *Mon. Weather Rev., 121*, 2351-2354, 1993.

Chiu, L.S., G.R. North, D.A. Short, and A. McConnell, Rain estimation from satellites: Effect of finite field of view, *J. Geophys. Res., 95*, 2177-2185, 1990.

Chiu, L.S., A. Chang, and J. Janowiak, Comparison of monthly rain rates derived from GPI and SSM/I using probability functions, *J. Appl. Meteorol., 32*, 323-334, 1993.

Dorman, C.E., and R.H. Bourke, Precipitation over the Pacific ocean, 30°S to 60°N, *Mon. Weather Rev., 107*, 896-910, 1979.

Dorman, C.E., and R.H. Bourke, Precipitation over the Atlantic ocean, 30°S to 70°N, *Mon. Weather Rev., 109*, 554-563, 1981.

Grody, N., Classification of snow cover and precipitation using the special sensor microwave/imager, *J. Geophys. Res., 96*, 7423-7435, 1991.

Jaeger, L., *Monthly and Areal Patterns of Mean Global Precipitation, Variations in the Global Water Budget*, 129pp., D. Reidel, Norwell, Mass., 1983.

Janowiak, J.E., P.A. Arkin, P. Xie, M.L. Morrissey, and D.R. Legates, An examination of the east Pacific ITCZ rainfall distribution, *J. Clim., 8*, 2810-2823, 1995.

Jones, D.M.A., and A.L. Sims, Climatology of instantaneous rainfall rates, *J. Appl. Meteorol., 17*, 1135-1140, 1978.

Kummerow, C., and L. Giglio, A passive microwave technique for estimating rainfall and vertical structure information from space, I, Algorithm description, *J. Appl. Meteorol., 33*, 3-18, 1994a.

Kummerow, C., and L. Giglio, A passive microwave technique for estimating rainfall and vertical structure information from space, II, Applications to SSM/I Data, *J. Appl. Meteorol., 33*, 19-34, 1994b.

Kummerow, C., R.A. Mack, and I.M. Hakkarinen, A self-consistency approach to improve microwave rainfall rate estimation from space, *J. Appl. Meteorol., 28*, 869-884, 1989.

Legates, D.R., and C.J. Willmott, Mean seasonal and spatial variability in gauge-corrected, global precipitation, *Int. J. Climatol., 10*, 111-127, 1990.

Liebe, H.J., An updated model for millimeter wave propagation in moist air, *Radio Sci., 20*, 1069-1089, 1985.

Lin, B., Observations of cloud water path and precipitation over oceans using ISCCP and SSM/I data, Ph.D. dissertation, Dep. of Geol. Sci., Columbia Univ., New York, 1995.

Lin, B., and W.B. Rossow, Observations of cloud liquid water path over oceans: Optical and microwave remote sensing methods, *J. Geophys. Res., 99*, 20907-20927, 1994.

Lin, B., and W.B. Rossow, Seasonal variation of liquid and ice water path in non-precipitating clouds over oceans, *J. Clim., 9*, 2890-2902, 1996.

Liu, G., and J.A. Curry, Retrieval of precipitation from satellite microwave measurements using both emission and scattering, *J. Geophys. Res., 97*, 9959-9974, 1992.

Liu, G., and J.A. Curry, Determination of characteristic features of cloud liquid water from satellite microwave measurements, *J. Geophys. Res., 98*, 5069-5092, 1993.

Liu, G., and J.A. Curry, Precipitation characteristics in the GIN seas determined using satellite microwave data, *J. Geophys. Res.*, in press, 1996.

Liu, G., J.A. Curry, and M. Weadon, Atmospheric water balance in typhoon Nina as determined from SSM/I satellite data, *Meteorol. Atmos. Phys., 54*, 141-156, 1994.

Marshall, J.S., and W.M. Palmer, The distribution of raindrops with size, *J. Meteorol., 5*, 165-166, 1948.

McClatchey, R.A., R.W. Fenn, J.E.A. Selby, F.E. Voltz, and J.S. Garing, Optical properties of the atmosphere, *Environ. Res. Pap. 411*, U.S. Air Force Cambridge Res. Lab., Bedford, Mass., 1972.

McGuirk, J.P., A.H. Thompson, and J.R. Shaefer, An eastern Pacific tropical plume, *Mon. Weather Rev., 116*, 2505-2521, 1988.

Minnis, P., P.W. Heck D.F. Young, C.W. Fairall, and J.B. Snider, Stratocumulus cloud properties derived from simultaneous satellite and island-based instrumentation during FIRE, *J. Appl. Meteorol., 31*, 317-339, 1992.

Morrissey, M.L., and J. Janowiak, Sampling-induced conditional biases in satellite climate-scale rainfall estimates, *J. Appl. Meteorol., 35*, 541-548, 1996.

Morrissey, M.L., M.A. Shafer, S.E. Postawko, and B. Gibson, The

Pacific rain gauge rainfall database, *Water Resour. Res., 31*, 2111-2113, 1995.

Mugnai, A., E.A. Smith, and G.J. Tripoli, Foundations for statistical-physical precipitation retrieval from passive microwave satellite measurements, II, Emission-source and generalized weighting-function properties of a time dependent cloud radiation model, *J. Appl. Meteorol., 32*, 17-39, 1993.

Negri, A.J., R.F. Adler, E.J. Nelki, and G.J. Huffman, Regional rainfall climatologies derived from special sensor microwave/imager (SSM/I) data, *Bull. Am. Meteorol. Soc., 75*, 1165-1182, 1994.

Olson, W.S., Estimation of rainfall rates in tropical cyclones by passive microwave radiometry, Ph.D. thesis, 292 pp., Univ. of Wis., Madison, 1987.

Paluch, I.R., and D.H. Lenschow, Stratiform cloud formation in the marine boundary layer, *J. Atmos. Sci., 48*, 2141-2158, 1991.

Parrish, J.L., and A.J. Heymsfield, A user guide to a particle-growth and trajectory model (using one-dimensional and three-dimensional wind fields), *NCAR Tech. Note NCAR/TN-259+IA*, 69 pp., Natl. Cent. for Atmos. Res., Boulder, Colo., 1985.

Petty, G.W., On the response of the special sensor microwave/imager to the marine environment--Implications for atmospheric parameter retrievals, Ph.D. dissertation, Dep. of Atmos. Sci., Univ. of Washington, Seattle, 1990.

Petty, G.W., Physical retrievals of over-ocean rain rate from multichannel microwave imagery, I, Theoretical characteristics of normalized polarization and scattering indices, *Meteorol. Atmos. Phys., 54*, 79-99, 1994a.

Petty, G.W., Physical retrievals of over-ocean rain rate from multichannel microwave imagery, II, Algorithm implementation, *Meteorol. Atmos. Phys., 54*, 101-121, 1994b.

Petty, G.W., Frequencies and characteristics of global oceanic precipitation from shipboard present-weather reports, *Bull. Am. Meteorol. Soc., 76*, 1593-1616, 1995.

Ray, P.S., Broadband complex refractive indices of ice and water, *Appl. Opt., 11*, 1836-1844, 1972.

Rossow, W.B., and R.A. Schiffer, ISCCP cloud data products, *Bull. Am. Meteorol. Soc., 72*, 2-20, 1991.

Short, D.A., and G.R. North, The beamfilling error in ESMR-5 observations of GATE rainfall, *J. Geophys. Res., 95*, 2187-2194, 1990.

Simpson, J.R., R.F. Adler, and G.R. North, A proposed tropical rainfall measuring mission (TRMM) satellite, *Bull. Am. Meteorol. Soc., 69*, 278-295, 1988.

Smith, E.A., and A. Mugnai, Radiative transfer to space through a precipitating cloud at multiple microwave frequencies, II, Results and analysis, *J. Appl. Meteorol., 27*, 1074-1091, 1988.

Smith, E.A., and A. Mugnai, Radiative transfer to space through a precipitating cloud at multiple microwave frequencies, III, Influence of large particles, *J. Meteorol. Soc. Jpn., 67*, 739-755, 1989.

Smith, E.A., A. Mugnai, H.J. Cooper, G.J. Tripoli, and X. Xiang, Foundations for statistical-physical precipitation retrieval from passive microwave satellite measurements, I, Brightness-temperature properties of a time dependent cloud-radiation model, *J. Appl. Meteorol., 31*, 506-531, 1992.

Spencer, R.W., Global oceanic precipitation from the MSU during 1979-91 and comparisons to other climatologies, *J. Clim., 6*, 1301-1326, 1993.

Spencer, R.W., H.M. Goodman, and R.E. Hood, Precipitation retrieval over land and ocean with the SSM/I: Identification and characteristics of the scattering signal, *J. Atmos. Oceanic Technol., 6*, 254-273, 1989.

Tsang, L., and J.A. Kong, Theory for thermal microwave emission from a bounded medium containing spherical scatterers, *J. Appl. Phys., 48*, 3593-3599, 1977.

Warren, S.G., Optical constants of ice from the ultraviolet to the microwave, *Appl. Opt., 23*, 1206-1255, 1984.

Wilheit, T.T., A.T.C. Chang, M.S.V. Rao, E.B. Rodgers, and J.S. Theon, A satellite technique for quantitatively mapping rainfall rates over the oceans, *J. Appl. Meteorol., 16*, 551-560, 1977.

Wilheit, T.T., A.T.C. Chang, and L.S. Chiu, Retrieval of monthly rainfall indices from microwave radiometric measurements using probability distribution functions, *J. Atmos. Oceanic Technol., 8*, 118-136, 1991.

Wu, R., and J.A. Weinman, Microwave radiances from precipitating clouds containing aspherical ice, *J. Geophys. Res., 89*, 7170-7178, 1984.

Yeh, H.-Y.M., N. Prasad, R.A. Mack, and R.F. Adler, Aircraft microwave observations and simulations of deep convection from 18 to 183 GHz., II, Model results, *J. Atmos. Oceanic Technol., 7*, 392-410, 1990.

B. Lin, NASA Langley Research Center, Mail Stop 420, Hampton, VA 23681-0001. (e-mail: bing@front.larc.nasa.gov)

W. B. Rossow, NASA Goddard Institute for Space Studies, 2880 Broadway, New York, NY 10025. (e-mail: clwbr@giss.nasa.gov)

(Received April 22, 1996; revised November 18, 1996; accepted November 18, 1996.)